Hulley, G.C., S.J. Hook, and A.M. Baldridge, 2008, ASTER Land Surface Emissivity Database of California and Nevada, Geophysical Research Letters, v. 35, L13401, doi:10.1029/2008GL034507. To view the published open abstract, go to **http://dx.doi.org** and enter the DOI.

GEOPHYSICAL RESEARCH LETTERS, VOL. ???, XXXX, DOI:10.1029/,

The ASTER Land Surface Emissivity Database of California and Nevada

G. C. Hulley

Jet Propulsion Laboratory, California Institute of Technology, Pasadena,

CA, USA

S. J. Hook

Jet Propulsion Laboratory, California Institute of Technology, Pasadena,

CA, USA

A. M. Baldridge

Jet Propulsion Laboratory, California Institute of Technology, Pasadena,

CA, USA

G. C. Hulley, Jet Propulsion Laboratory, 4800 Oakwood drive, Pasadena, CA, USA.

(glynn.hulley@jpl.nasa.gov)

Land surface temperature and emissivity (LST&E) are essential parameters for a wide range of studies undertaken at a variety of spatial scales. LST&E products are generated by a number of spaceborne sensors such as ASTER, MODIS, and AIRS at varying spatial, spectral and temporal resolutions. We have developed an approach for producing gridded, mean, seasonal ASTER LST&E Datasets at a spatial resolution of 100 m at nadir. We have produced a mean wintertime and summertime emissivity dataset for California and Nevada, USA using all available data since mission launch (2000). Comparison of the two seasonal datasets indicates the greatest variability occurs in areas affected by snow such as the Sierra Nevada Mountains, and in agricultural regions. Comparisons of the new emissivity dataset with laboratory measurements of geologic samples show emissivity differences of less than 0.5%, while 1- 3% differences were found for water and vegetation using spectra from the MODIS UCSB library.

1. Introduction

One of the most important Earth System Data Records (ESDR's) identified by NASA and numerous international organizations is Land Surface Temperature and Emissivity (LST&E) [*King*, 1999]. LST&E data are key parameters in the physics of climate modeling, ice dynamic analyses, surface-atmosphere interactions and land use, land cover change.

For example, emissivity is a critical component for climate and ecosystem models that determine surface radiation budget and energy flux calculations between the surface and the atmosphere. Furthermore, knowledge of the surface emissivity is needed to recover the Land Surface Temperature (LST), an important climate variable in many scientific studies from climatology to hydrology and modeling the greenhouse effect. Sensitivity tests indicate that a decrease of soil emissivity by 0.1 will result in current climate models having errors of up to 6.6 Wm^{-2} in upward longwave radiation for their surface energy budget in arid and semi-arid regions [*Zhou et al.*, 2003a; *Jin and Lang*, 2006]. This represents a much larger term than, for example, surface radiative forcing due to greenhouse gases.

The atmospheric retrieval community and numerical weather prediction operational centers are expected to benefit from an improved emissivity product from ASTER. For example, using constant or inaccurate surface emissivities typically results in large temperature and moisture profile errors, particularly over desert and semi-arid regions where the variation in emissivity is both large spatially and spectrally [*Li et al.*, 2007]. By producing a more accurate emissivity product, along with an error estimate at high resolution, we aim to minimize what would normally be a major source of error and bias in retrieval schemes and the use of satellite radiances in data assimilation.

ASTER has acquired the necessary data to produce a global, gridded high spatial resolution LST&E dataset. To accomplish this, we use current ASTER LST&E products (AST_05 and AST_08) provided on a scene-by-scene basis using the Temperature Emissivity Separation (TES) algorithm [*Gillespie et al.*, 1999]. TES uses an empirical relationship to predict what the minimum emissivity would be from the observed spectral contrast [*Kealy and Hook*, 1993; *Matsunaga*, 1994] using a calibration curve derived from a subset of the ASTER spectral library. TES can recover temperatures within 1.5 K and emissivities within 0.015 for a wide range of surfaces. The limitations in the TES algorithm arise from three sources; reliance on an empirical function, inaccurate atmospheric corrections, and errors in radiometric calibration of the TIR channels. Two parameter changes were made to the TES algorithm on August 1st, 2007 as discussed in *Gustafson et al.*, (2006). The first removed a threshold classifier for low spectral contrast features (water, vegetation) that resulted in artificial step discontinuities in a small fraction of ASTER images, and the second removed the iterative correction for reflected downwelling irradiance resulting in improved spectral shape and performance. The consequence of the first change was a smoother appearance for all images, but at the cost of TES underestimating emissivity of graybody scenes such as water by up to 3%, and vegetation by up to 2%.

Using the results from TES, we have produced two seasonal, mean LST&E datasets, covering the months Jan-Feb-Mar (wintertime) and Jul-Aug-Sep (summertime). In these seasonal datasets, the emissivity is calculated as the average emissivity of all clear-sky pixels for a given location from all scenes acquired in the season over the entire period of acquisition of ASTER data (2000-2008). The methodology is now discussed together with an evaluation of the seasonal datasets for California and Nevada and a validation of this dataset.

2. Methodology

In order to distinguish between clear and cloudy pixels, a New ASTER Cloud Mask Algorithm (NACMA) was developed [*Hulley and Hook*, 2008]. Using the cloud-mask algorithm, it was possible to download all the data for a given location (clear and cloudy), and then use the mask in an automated fashion to identify any clear pixels for subsequent use. The cloud mask utilizes a variety of spectral tests based on the Landsat-7, MODIS and AVHHR cloud assessment schemes and is produced at high resolution (100 m). The new cloud mask has been tested over a variety of different conditions and scene types and shows significant improvement over the original ASTER L1A cloud mask, particularly in detecting cirrus over snow/ice scenes.

The ASTER Land Surface Emissivity Aggregation Algorithm (ALSEA) was developed to produce the gridded dataset. ALSEA processes any number of input ASTER LST&E scenes (AST_05 and AST_08) and computes the mean and standard deviation for each pixel on a gridded data set. The algorithm has three distinctive components: 1) a cloud mask is generated using NACMA and saved for each scene; 2) the cloud mask is applied and all intersecting scenes are 'stacked' on 0.5° (~50 km) grid-boxes at 100 m resolution; 3) the mean and standard deviation are computed for all observations on each pixel on the grid-box.

Furthermore, an outlier test is included that removes any spurious data that can result from lack of convergence of the TES algorithm, a bad atmospheric correction, or from undetected cirrus. The outlier test uses the inter-quartile range (IQR) as a measure of statistical dispersion which represents the range of the middle 50% of the data. Values that fall above or below 1.5*IQR of the 75th and 25th percentile values are considered outliers and are rejected. The outlier test is engaged when there are a minimum of 5 samples per pixel, and for the California-Nevada area, this represents ~90% of all pixels. ASTER data are collected episodically with a repeat cycle of 16 days, and this occasionally results in ‘streaking’ between very low and very high data coverage regions - a limitation of this dataset.

Our approach of ‘stacking’ multiple scenes together for a given area and computing mean values over long time periods maximizes the use of the available data for our purpose of generating global, gridded surface datasets compared with the traditional mosaicking methods that attempt to seamlessly blend together overlapping scenes for short time periods and small test areas. The traditional mosaicing approach works well for short periods over areas with good coverage but provides an inconsistent product when applied to larger areas over extended time periods. Examples of this approach include the work by *Scheidt et al.* [2007] to study dune fields and sand sheets in the Gran Desierto area in Mexico and also by *Ogawa et al.* [2003] to estimate land surface window emissivity (8 - 12 μm) in a portion of the Sahara desert.

3. Results

3.1. Seasonal Emissivity Differences

In order to evaluate ALSEA we have produced seasonal, gridded emissivity datasets for California and Nevada using all the available daytime ASTER scenes from 2000-2008 for the winter (Jan-Feb-Mar) and summer (Jul-Aug-Sep). The states of California and Nevada provide an excellent test case since they encompass a broad range of emissivities and cover types from low values in the quartz-rich desert areas of southwestern California, to high values over the northern California forests. In general, the summertime emissivity dataset should correspond to the time of maximum vegetation cover and therefore highest emissivity, while the wintertime emissivity datasets should correspond to minimum vegetation cover (maximum soil exposure) and therefore minimum emissivity. The two seasonal end-member emissivity datasets typically encompass the maximum emissivity range expected for any given location, and the maximum standard deviation within each season. For example, during the summer in agricultural regions we should expect to see some variability since crop fields may be vegetated in some years and fallow in others. Emissivity in desert regions will also change due to variations in soil moisture and vegetation cover. Given both the mean and standard deviation we can say not only what the mean seasonal emissivity value is for a specific location but also how much range is expected in that emissivity value before it becomes unrealistic.

A total of 3,102 summer and 2,617 winter ASTER scenes were processed for California- Nevada using NACMA and ALSEA. Figure 1 shows the mean summer emissivity map of California and Nevada for band 11 (8.6 μm) at 1 km spatial resolution (for plotting purposes) and Figure 2 shows the difference between the mean summer and mean winter emissivity product. Generally the emissivity differences between the summer and winter area are very small, typically between +-0.01 emissivity units which corresponds to a temperature error of 0.7 K for a material at 300 K and a wavelength of 8.6 μm. However there are areas which show large variations of up to 0.1 units, for example the Sierra Nevada Mountains in California (Figure 2-A) and the Schell Creek and Snake Ranges in Nevada (Figure 2-B) show large negative differences as a result of increased snow cover and therefore higher emissivity values during the winter months than the summer months when there is more rock or soil exposure. Areas over the Central (Figure 2-C) and Salinas Valleys (Figure 2-D) have large positive differences of up to 0.05 units indicating higher emissivities during the summer months due to more intensive agricultural practices. This is particularly evident over Kings County, a rich agricultural region where almost 70% of land use is reserved for crops, vineyards and orchards. Conversely, the Coachella and Imperial valleys just north and south of the Salton Sea (Figure 2-E) are also intensive agricultural regions, but have small negative emissivity differences from summer to winter. This is because crops in this area are grown all year round as a result of the extreme heat during the summer months. Also interesting to note is that Honey Lake (Figure 2-F) shows large, positive differences as a result of fluctuating water levels and the associated drying out of its margin during extended periods of drought.

3.2. Validation Results

In order to validate the new emissivity dataset, the emissivities of selected regions were compared with the emissivity of field samples and spectral libraries. Spectral library measurements included samples of water and vegetation from the MODIS UCSB Emissivity Library (http://www.icess.ucsb.edu/modis/EMIS/html/em.html). For the field samples, 10 samples were taken from the quartz-rich Algodones dunes on the far southeast corner of California (Figure 1-B), and 10 samples were taken from a carbonate-rich alluvial fan at Cuprite, NV (Figure 1-A). The Algodones dunes cover an area of roughly 13 by 64 kilometers and are very homogeneous. The carbonate alluvial fan covers an area of roughly 2 by 1 kilometers. The directional hemispherical reflectance of the field samples was measured using the JPL Fourier Transform Infrared Spectrometer, converted to emissivity using Kirchhoff's law, and convolved to the ASTER spectral response functions. The field samples were collected at intervals of approximately 250 m covering a grid of approximately 500 m^2 at each site. Emissivities from the new dataset where then extracted covering a 2x2 pixel area (200 m^2) around each of the sampling areas for the comparisons. Figure 3 shows a 1° x 1° area of emissivity from band 11 (8.6 μm) around each of the sampling sites. Areas at each site where ASTER emissivities were extracted are marked with black X's. Figure 4 shows the comparisons between ASTER and the laboratory results for each of the sites. The emissivity mean and standard deviation (errorbar) are shown at each ASTER wavelength for the total number of samples and pixels used. There is excellent agreement between the ASTER and laboratory results for both geologic samples. The Cuprite carbonates agree to within 0.4% in all bands except band 12 (9.1 μm) which shows a difference of 1.4%. The Algodones quartz samples agree to within 0.5% for bands 10-13 but have a difference of up to 2% in band 14. The cause for the large difference in band 14 is still unclear and was also observed by *Schmugge et al.* (2003).

The emissivity of a 5*x*5 pixel area centered on Lake Tahoe was then compared with the emissivity of distilled water from the MODIS UCSB library (Figure 1-C). The comparisons show ASTER underestimates the emissivity of water between 2-3% in all bands. This underestimation (bias) arises due to changes in the TES algorithm discussed in the Introduction. The emissivity of a 5*x*5 pixel area corresponding to a dense stand of conifers in Redwood National Park in northernwestern California (Figure 1-D) was compared to the emissivity spectra of a pine needle sample (conifer) from the MODIS UCSB library. The differences range from 1-2% and again can be attributed to TES underestimating the emissivity of low spectral contrast surfaces. It should also be noted that leaf/pine-needle samples measured in the lab may not accurately represent the canopy scattering effects of natural forested areas.

4. Conclusions

We have developed an approach for producing a high spatial resolution, mean, gridded emissivity product from ASTER data and demonstrated the approach by producing the first such land surface emissivity dataset for California and Nevada. The ASTER Land Surface Emissivity Aggregation Algorithm (ALSEA) along with a New ASTER Cloud Mask Algorithm (NACMA) were developed specifically for this task and in combination are able to assimilate any given number of input ASTER scenes whether clear or cloudy. The output product consists of the mean and standard deviation of land surface emissivity (all TIR bands) and temperature in 1° grid-boxes at 100 m spatial resolution for summer (Jul-Aug-Sep) and winter (Jan-Feb-Mar). Seasonal emissivity differences indicate the greatest variability occurs in areas affected by snow such as the Sierra Nevada Mountains and in agricultural regions such as the Central Valley. Initial validation of the new emissivity dataset shows promising results for carbonate and quartz-rich samples collected in Cuprite, NV and Algodones dunes, CA with differences of less than 0.5% when compared to laboratory results. The emissivity of low-contrast spectral surfaces (water, vegetation) on the other hand are underestimated by 1-3% due to limitations of the TES algorithm.

Acknowledgments. The research described in this paper was carried out at the Jet Propulsion Laboratory, California Institute of Technology, under a contract with the National Aeronautics and Space Administration.

References

Abdalati, W. and K. Steffen (2001), Greenland ice sheet melt extent: 1979-1999, *J. Geophys. Res.*, 106(D24):33, 983-33, 989.

Gillespie, A., S. Rokugawa, T. Matsunaga, S. Cothern, S. Hook, and A. Kahle, (1999), The ASTER Temperature/Emissivity Separation Algorithm Theoretical Basis Document (ATBD-AST-03).

Gustafson, W. T., A. R Gillespie, and G. J. Yamada, (2006), Revisions to the ASTER temperature/emissivity separation algorithm, 2nd International Symposium on Recent Advances in Quantitative Remote Sensing, 25-29th September 2006, Torrent (Valencia), Spain.

Hall, D. K., R. S. Williams, Jr. and N. E. DiGirolamo, submitted: Greenland Ice Sheet surface temperature and melt variability, 2000-2006.

Hulley, G. C. and S. J. Hook (2008), A New Methodology for Cloud Detection and Classification with Advanced Spaceborne Thermal Emission and Reflection (ASTER) Data, *Geophys. Res. Lett.*, in review

Jin, Menglin and S. Liang (2006), Improving land surface emissivity parameter of land surface models in GCM, *J. Clim.*, *19*, 2867-2881, 2006.

Kealy P. S. and S. Hook, (1993), Separating temperature and emissivity in thermal Infrared multispectral scanner data: Implication for recovering land surface temperatures, *IEEE Trans. Geosci. Remote Sens.*, *31*, 1155-1164.

King, M. D. (1999), EOS Science Plan: The State of Science in the EOS.

Krabill, W. E., P. Hanna, W. Huybrechts, J. Abdalati, B. Cappelen, E. Csatho, S. Frederick, C. Manizade, J. Martin, R. Sonntag, R. Swift, W. Thomas, and J. Yungel (2004), Greenland Ice Sheet: Increased coastal thinning, *Geophys. Res. Lett.*, *31*, L24402, doi:10/1029/2004GL021533.

Li J., J. Li, E. Weisz, and D. K. Zhou (2007), Physical retrieval of surface emissivity spectrum from hyperspectral infrared radiances, *Geophys. Res. Lett.*, *34*, L16812, doi:10.1029/2007GL030543

Matsunaga, T., (1994), A temperature-emissivity separation method using an empirical relationship between the mean, the maximum, and the minimum of the thermal infrared emissivity spectrum, in Japanese with English abstract, *J. Rem. Sens. Soc. Japan*, vol. 14, no. 2, pp. 230-241.

Ogawa, K., T. Schmugge, F. Jacob, and A. French (2003), Estimation of land surface window (8-12 μm) emissivity from multi-spectral thermal infrared remote sensing - A case study in a part of Sahara Desert, *Geophys. Res. Lett.*, *30(2)*, 1067, doi:10.1029/2002GL016354.

Scheidt, S., M. S. Ramsey, and N. Lancaster (2007), Image mosaic generation of ASTER thermal infrared data: An application to extensive sand sheets and dune fields, *Rem. Sens. Environ. (in press)*

Zhou, L., R. E. Dickinson, Y. Tian, M. Jin, K. Ogawa, H. Yu, and T. Schmugge (2003a), A sensitivity study of climate and energy balance simulations with use of satellite derived emissivity data over the northern Africa and the Arabian peninsula, *J. Geophys. Res.*, *108(D24)*, 4795, doi:10.1029/2003JD004083

Caption 1

Mean emissivity map of California and Nevada for band 11 (8.6 μm) during the summer (Jul-Aug-Sep) at 1 km spatial resolution. Areas A, B, C and D show validation site areas in Figures 3 and 4.

Caption 2

Seasonal emissivity difference map of California and Nevada (summer minus winter) for band 11 (8.6 μm) at 1 km spatial resolution. White areas within the border are areas with no clear-sky coverage during the winter period.

Caption 3

Four validation sites used in this study from clockwise top left; carbonate sediment - Cuprite, NV, quartz - Algodones dunes, CA, water - Lake Tahoe, CA, and conifer - Redwood National Park, CA. The plots show the mean summer emissivity at 8.6 μm, and X's mark the spot where pixels were extracted from the new ASTER emissivity dataset for the comparisons with laboratory measurements.

Caption 4

Corresponding Emissivity spectra for four sites in Figure 3 showing comparisons with the new ASTER emissivity dataset and results from the JPL-FTIR for geologic samples collected at Cuprite and Algodones dunes (top two panels), and from water and vegetation spectra taken from the MODIS UCSB spectral library (bottom two panels).

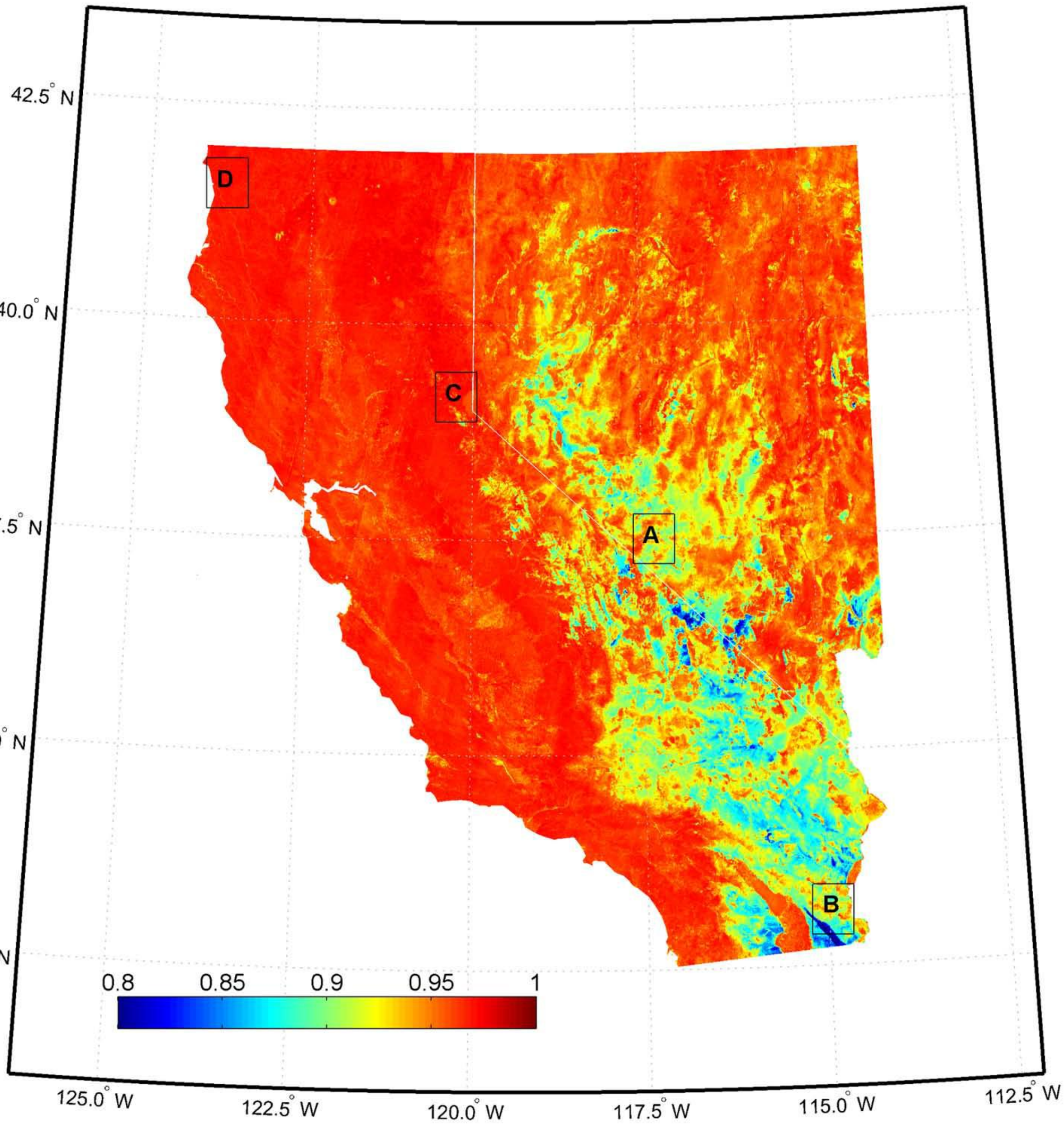
42.5° N
40.0° N
37.5° N
35.0° N
32.5° N
125.0° W
122.5° W
120.0° W
117.5° W
115.0° W
112.5° W
D
C
A
B
0.8
0.85
0.9
0.95
1

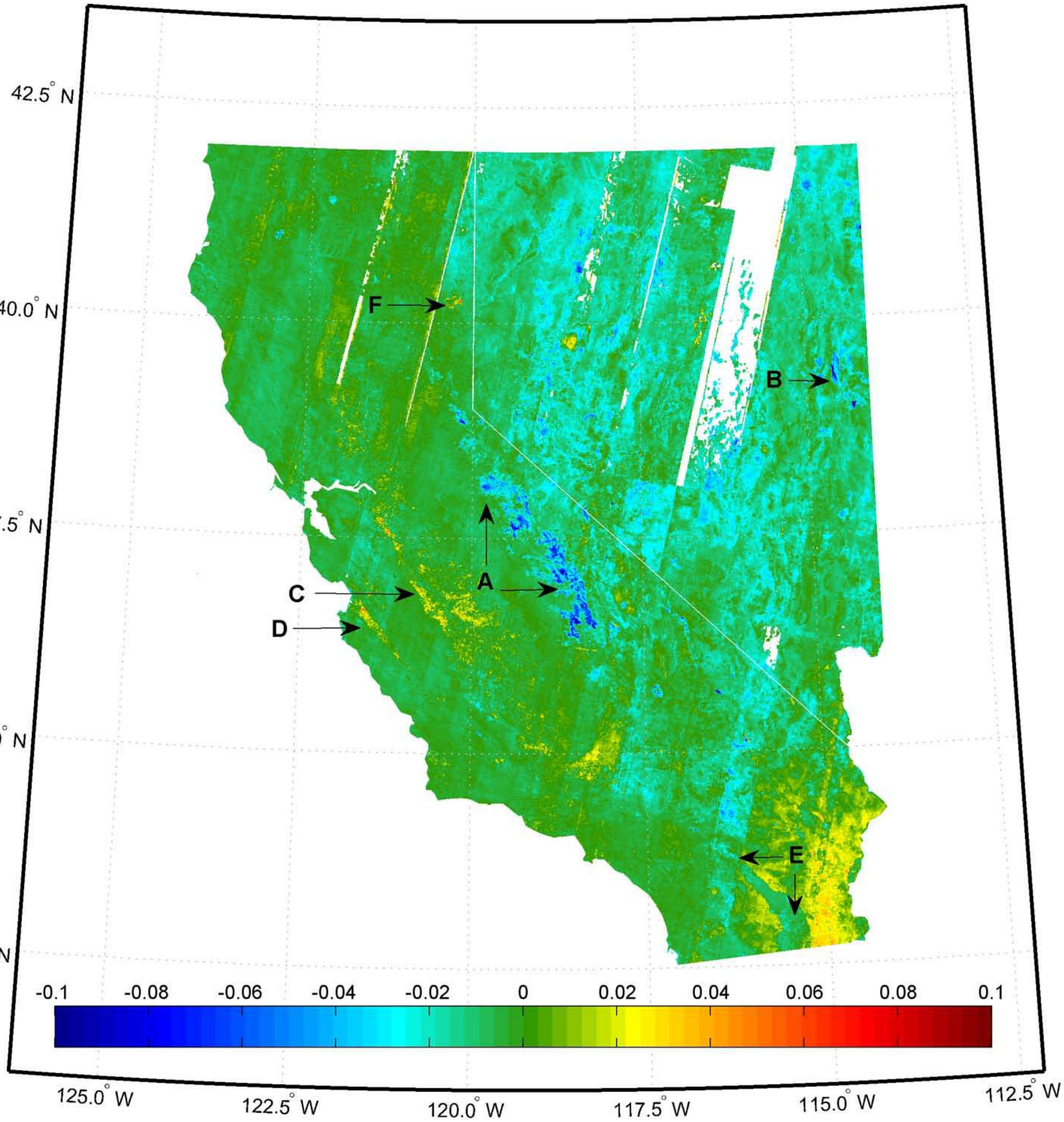
42.5° N
40.0° N
37.5° N
35.0° N
32.5° N
A
B
C
D
E
F
-0.1
-0.08
-0.06
-0.04
-0.02
0
0.02
0.04
0.06
0.08
0.1
125.0° W
122.5° W
120.0° W
117.5° W
115.0° W
112.5° W

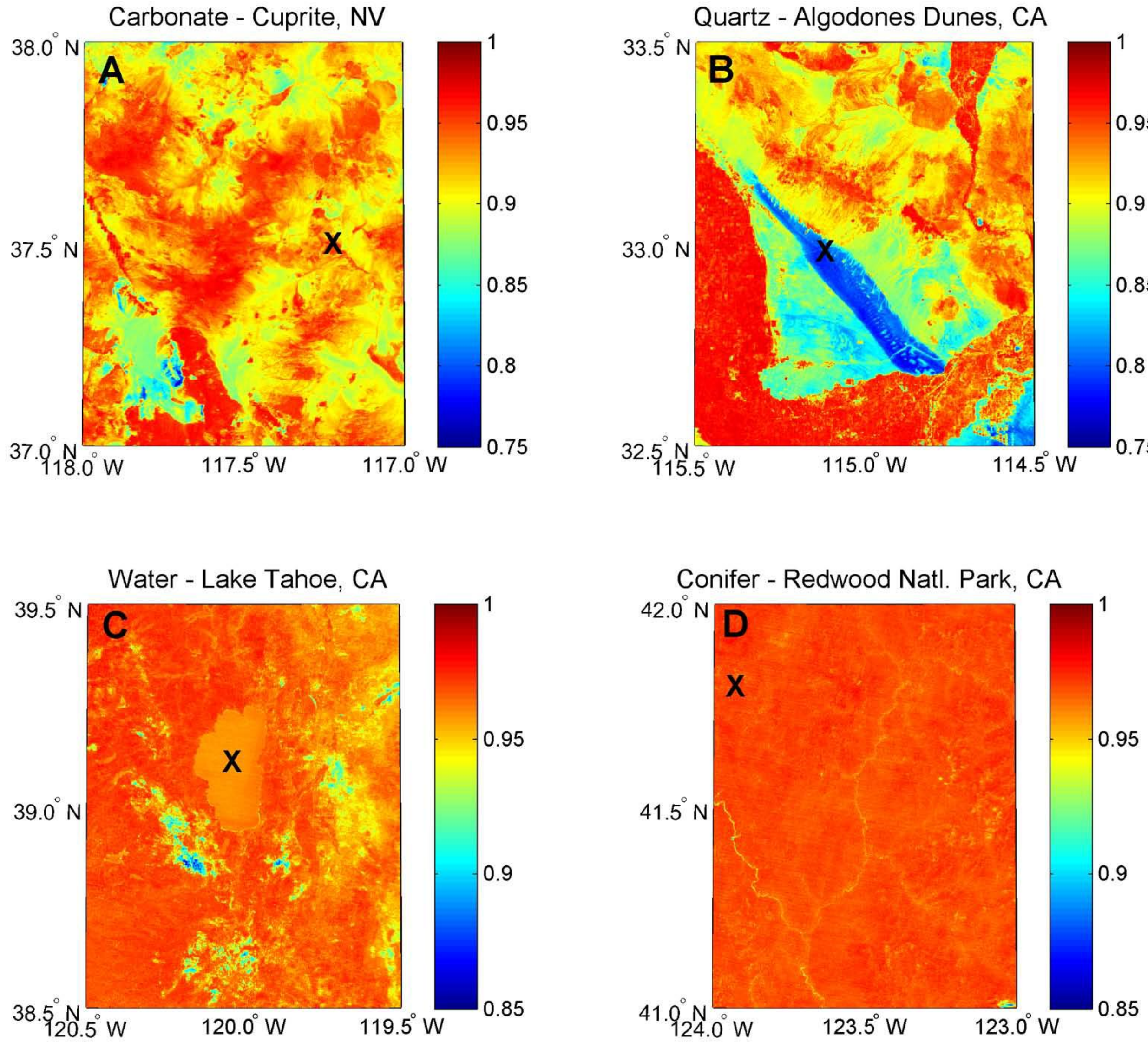
Carbonate - Cuprite, NV
A
X
38.0° N
37.5° N
37.0° N
118.0° W
117.5° W
117.0° W
1
0.95
0.9
0.85
0.8
0.75
Quartz - Algodones Dunes, CA
B
X
33.5° N
33.0° N
32.5° N
115.5° W
115.0° W
114.5° W
1
0.95
0.9
0.85
0.8
0.75
Water - Lake Tahoe, CA
C
X
39.5° N
39.0° N
38.5° N
120.5° W
120.0° W
119.5° W
1
0.95
0.9
0.85
Conifer - Redwood Natl. Park, CA
D
X
42.0° N
41.5° N
41.0° N
124.0° W
123.5° W
123.0° W
1
0.95
0.9
0.85

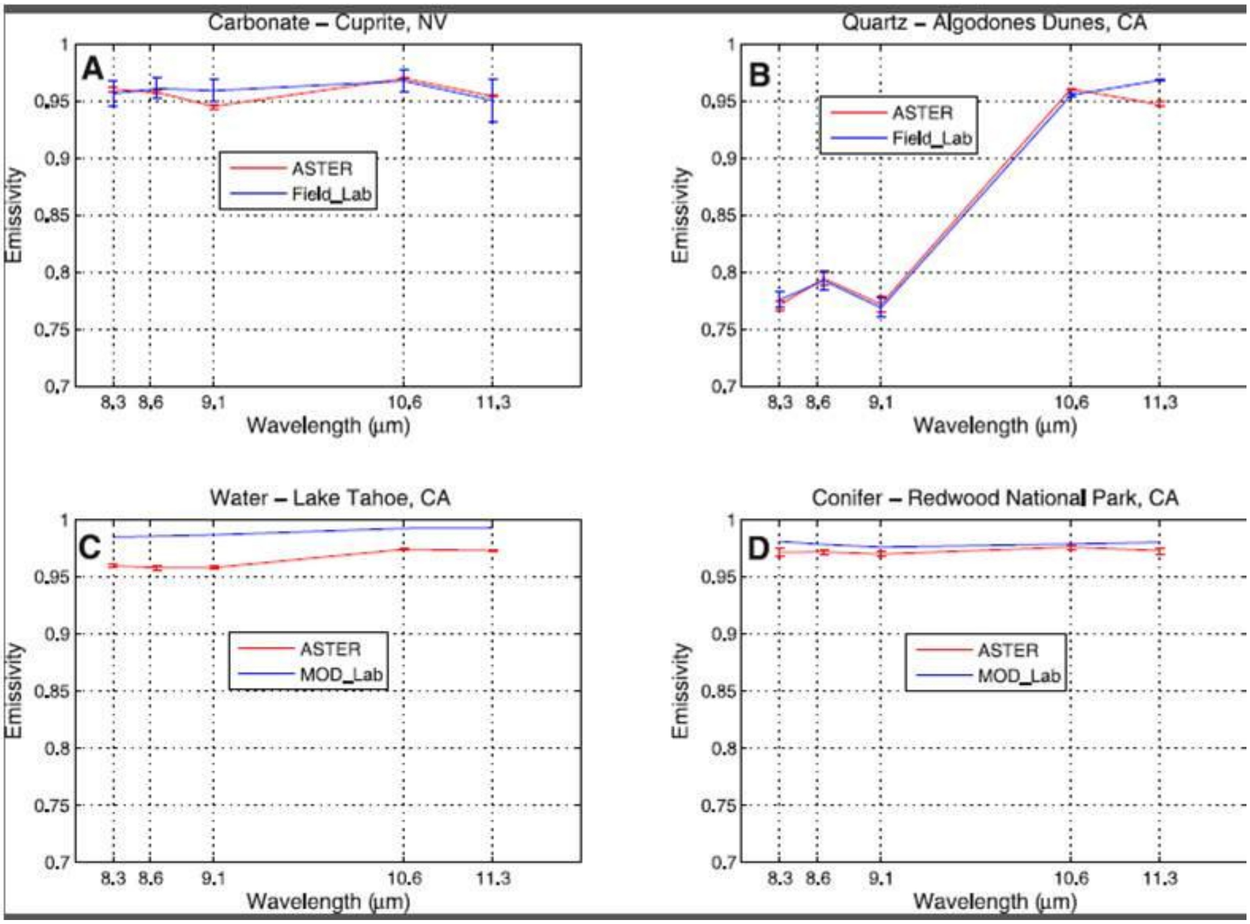
Carbonate – Cuprite, NV
A
ASTER
Field_Lab
Emissivity
Wavelength (μm)
Quartz – Algodones Dunes, CA
B
ASTER
Field_Lab
Emissivity
Wavelength (μm)
Water – Lake Tahoe, CA
C
ASTER
MOD_Lab
Emissivity
Wavelength (μm)
Conifer – Redwood National Park, CA
D
ASTER
MOD_Lab
Emissivity
Wavelength (μm)